

Incoherent cross-correlation spectroscopy

P. Tong, K.-Q. Xia,^{a)} and B. J. Ackerson

Department of Physics, Oklahoma State University, Stillwater, Oklahoma 74078

(Received 4 February 1993; accepted 4 March 1993)

A new light scattering method is developed to measure scattering amplitude fluctuations resulting from either internal motions of flexible macromolecules or rotations of rigid particles. With a single-beam two-color cross-correlation scheme, the technique becomes insensitive to rapid phase fluctuations of the scattered light produced by translational motions of the scattering particles. We frame the scattering theory so as to encompass rotations and number fluctuations of small particles in a steady laminar flow. Experiment verifies the theory and demonstrates its applications. The technique can be used to measure the magnitudes of the local velocity and the flow vorticity. It can also be used to measure internal motions and shape fluctuations of flexible macromolecules. The advantages of the technique are its high spatial resolution, fast temporal response, and ease of use.

I. INTRODUCTION

In recent years there is a growing interest in studying internal motions and shape fluctuations of polymer molecules,¹ microemulsion droplets,² and other flexible macromolecules or aggregates.³ Many experimental and theoretical investigations also focus on rotational dynamics of small particles in concentrated colloidal suspensions^{4,5} and in hydrodynamic flows.⁶ A variety of experimental methods have been used to measure the time dependence of thermal and hydrodynamic fluctuations in these systems, and one of the most popular methods is the homodyne autocorrelation spectroscopy (HS).^{7,8} With the HS scheme one scatters a monochromatic laser light from particles suspended in a fluid (e.g., colloidal particles, polymer molecules, or some self-assembly aggregates). These particles scatter light while undergoing Brownian motion or following local flow. A photodetector records the scattered light intensity $I(t)$, which fluctuates due to the motion of the particles. The frequencies of the fluctuating intensity can be obtained from the intensity autocorrelation function⁷ $g_a(t) = \langle I(t'+t)I(t') \rangle / \langle I(t') \rangle^2$. Here the angle brackets represent a time average over t' .

The correlation function $g_a(t)$ is most sensitive to the relative particle translational motions, which result in rapid phase fluctuations of the total scattering field due to the interference between the coherent fields scattered by different moving particles. When the particles are optically anisotropic, their internal motions or rotations can produce additional amplitude fluctuations of the scattering field. The measured $g_a(t)$ then becomes a product of two correlation functions; one is for the amplitude fluctuations of the scattered field and the other is for the phase fluctuations. In order to use the HS method to probe the scattering amplitude fluctuations, one has to know exactly the particle translational motions. In addition, the experimental situation is sometimes complicated by the fact that the

decay of $g_a(t)$ is usually dominated by the rapid phase fluctuations of the scattered light.

In this paper we report a new scattering method, which measures only the frequency spectrum of the scattering amplitude fluctuations. To accomplish this an incoherent light detecting method is used in order to be insensitive to the rapid phase fluctuations produced by the relative Doppler shifts of the scattering particles. Experimentally, we measure the intensity cross-correlation function

$$g_c(t) = \frac{\langle I_b(t')I_g(t'+t) \rangle}{\langle I_b \rangle \langle I_g \rangle} = 1 + bG_c(t),$$

where I_b and I_g are the scattered intensities (for example, the blue light and the green light) from the same laser source, and b (≤ 1) is an instrumental constant which depends on the geometry of the experimental setup. Because there is no phase coherence between I_b and I_g , $g_c(t)$ is only sensitive to the scattering amplitude fluctuations. This method takes the advantages of a laser source while eliminating its coherence by using the two-color cross-correlation scheme. Under different sampling conditions, cross-correlation schemes have been used in studies of anticorrelations of light scattered by nonspherical particles,⁹ local structure in disordered phases,^{10,11} and suppression of multiple scattering effects in optically thick media.¹²⁻¹⁴

Our two-color cross-correlation scheme is capable of measuring the scattering amplitude fluctuations with a cut-off frequency up to 1 MHz and a spatial resolution better than 100 μm . The experimental uncertainties are essentially statistical. At a moderately high scattering intensity ($I \sim 10^4$ counts/s), it only takes ~ 10 min to collect the data with an adequate signal-to-noise ratio. Since an incoherent detecting method is used, an increasing number of particles in the scattering volume tends to average out the scattering amplitude fluctuations. In fact, as will be shown below, the function $G_c(t)$ goes as $1/N$, where N is the number of particles in the scattering volume. In a typical experimental arrangement the particle number in the scattering volume can be controlled in the range $1 < N < 100$, and therefore, the smallest signal-to-noise ratio [evaluated

^{a)}Also Department of Physics, The Chinese University of Hong Kong, Shatin, NT, Hong Kong.

by the value of $G_c(t)$ at time $t=0$] is at the 1% level. Because of the small signal-to-noise ratio, it is difficult to measure $g_c(t)$ using normal commercial correlators. The new correlator used in the experiment is the ALV-5000 multiple- τ correlator, which makes it much easier to probe incoherent fluctuations with small amplitudes and long relaxation times. The ALV-5000 correlator is capable of measuring fluctuating signals with a signal-to-noise ratio as low as 0.1%. It should be pointed out that the present technique is not meant to replace the homodyne or the heterodyne autocorrelation methods, rather, it should be used to complement these techniques. Unlike the autocorrelation function $g_a(t)$, the cross-correlation function $g_c(t)$ measures the frequency spectrum of scattering amplitude fluctuations without any contamination from translational motions of the probe particles. Our cross-correlation method is particularly useful to measure rotations of rigid particles and internal motions and shape fluctuations of flexible macromolecules in situations where either the particle translational motion is not known, or the fluctuation spectrum of the scattering intensity is dominated by the rapid phase fluctuations resulting from the particle translational motion.

The paper is organized as follows. First, we present the theoretical calculations necessary to measure the scattering amplitude fluctuations using incoherent cross-correlation spectroscopy. We consider two common sources which produce the scattering amplitude fluctuations: (1) rotations of optically anisotropic particles in a steady laminar flow and (2) particle number fluctuations in the scattering volume when a hydrodynamic flow is present. Second, we report experimental results which verify the method and illustrate its applications. A primary objective of the paper is to delineate the experimental conditions for the measurement of the cross-correlation function $g_c(t)$. In the experiment, the incoherent cross-correlation spectroscopy is first applied to study Brownian rotation of small rodlike particles in water. We then use the technique to study number fluctuations of small particles in a steady laminar flow. Our experiments illustrate that incoherent cross-correlation spectroscopy is a useful technique to measure the magnitudes of the local velocity and the flow vorticity. Although the present experiments are motivated by studies of hydrodynamic flows, we expect the technique of incoherent cross-correlation spectroscopy to be useful in the future for measuring the internal motions and shape fluctuations of flexible macromolecules. Measurements of the cross-correlation function $g_c(t)$ will yield information about the fluctuation spectrum of the internal modes³ of the molecules without predominant contributions from translational motions of these molecules.

II. THEORY

The basic dynamic light scattering theory for coherent and incoherent sources can be found in the literature.^{7,15} Here we review the theory so as to encompass rotations and number fluctuations of small particles in a steady laminar flow. In many cases rotational and translational diffusive motions of small probe particles suspended in a ther-

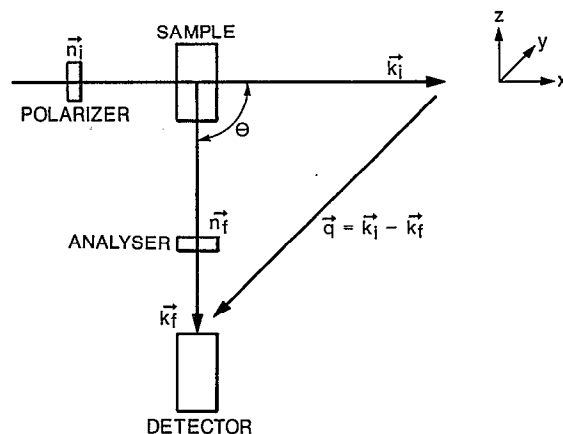


FIG. 1. Schematic diagram of the scattering geometry (z axis is perpendicular to the paper): \mathbf{k}_i , incident wave vector; \mathbf{k}_f , scattering wave vector; \mathbf{n}_i , \mathbf{n}_f , polarization directions of the polarizer and the analyzer; θ , scattering angle.

mal equilibrium solution (no hydrodynamic flow) serve as useful examples to test the theory and to calibrate the measurements. Therefore, Brownian motion of small seed particles is briefly discussed in the section as well.

A. Scattering from optically anisotropic particles

We consider the scattering by N identical particles, which scatter light anisotropically. Here the word “particles” refers to colloidal particles, polymer molecules, microemulsion droplets, and other flexible macromolecules or aggregates suspended in a solution. Composition fluctuations of fluid mixtures near the critical point may also be viewed as “scattering particles.” In the case where the polarization direction of the incident beam is perpendicular to the scattering plane, the total electric field, $E(t)$, is a simple sum of the fields radiated by each of the particles in the illuminated volume, and has the form⁷

$$E(t) = \sum_{j=1}^N \alpha_{if}^j(t) e^{-i\mathbf{q} \cdot \mathbf{r}_j(t)}, \quad (1)$$

where $\alpha_{if}(t) = \mathbf{n}_f \cdot \alpha(t) \cdot \mathbf{n}_i$ is the component of the molecular polarizability tensor $\alpha(t)$ along the incident polarization direction \mathbf{n}_i and the final scattered polarization direction \mathbf{n}_f , both of them being fixed in the laboratory. In Eq. (1) $\mathbf{r}_j(t)$ is the position of the center of mass of the j th particle at time t , \mathbf{q} is the photon momentum transfer vector to be defined below, and a proportionality constant has been omitted for simplicity.

Figure 1 shows a typical scattering geometry. The scattering plane is defined by the incident wave vector \mathbf{k}_i and the scattering wave vector \mathbf{k}_f . The polarization direction \mathbf{n}_f of the detected light can be either perpendicular to the scattering plane (the VV scattering geometry) or parallel to the scattering plane (the VH scattering geometry). The momentum transfer vector is $\mathbf{q} = \mathbf{k}_i - \mathbf{k}_f$, and its amplitude is $q = (4\pi n/\lambda) \sin(\theta/2)$, where θ is the scattering angle, n is the refractive index of the solvent, and λ is the wavelength of the incident light. The polarizability component $\alpha_{if}(t)$ varies in time either because of the rotations of the

particles or because of the internal motions of the particles if they are flexible. The phase factor $e^{-i\mathbf{q}\cdot\mathbf{r}(t)}$ changes with time since the particles move.

The cross-correlation function of the scattering light intensity is defined as

$$g_c(t) = \frac{\langle E_b^*(0)E_b(0)E_g^*(t)E_g(t) \rangle}{\langle E_b^*(0)E_b(0) \rangle \langle E_g^*(0)E_g(0) \rangle} = \frac{K}{Q_b Q_g}, \quad (2)$$

where the angle brackets represent the time average. In the simple case where the molecular polarizability tensor $\alpha(t)$ is independent of the wavelength of the incident light, we have $Q_b = Q_g = Q$, with

$$Q = \sum_{i,j}^N \langle \alpha_{if}^i(t) \alpha_{if}^j(t) \rangle \langle e^{-i\mathbf{q}\cdot[\mathbf{r}_i(t) - \mathbf{r}_j(t)]} \rangle = N \langle \alpha_{if}^2(t) \rangle. \quad (3)$$

In the above, we have assumed that the phase and the amplitude fluctuations of the scattered light are statistically independent. This decoupling approximation is valid because the time scales involved in the two processes are usually widely separated. The fluctuation terms ($i \neq j$) in Eq. (3) do not survive a time or ensemble average, because the particles are assumed to be randomly distributed in the fluid.

The function K in Eq. (2) has the form

$$K = \sum_{i,j,k,l}^N \langle \alpha_{if}^i(0) \alpha_{if}^j(0) \alpha_{if}^k(t) \alpha_{if}^l(t) \rangle \times \langle e^{-i[\mathbf{q}_b \cdot [\mathbf{r}_i(0) - \mathbf{r}_j(0)] + \mathbf{q}_g \cdot [\mathbf{r}_k(0) - \mathbf{r}_l(0)]]} \rangle \times \langle e^{-i\mathbf{q}_g \cdot \int_0^t dt' \{ \mathbf{v}[\mathbf{r}_k(t')] - \mathbf{v}[\mathbf{r}_l(t')] \}} \rangle, \quad (4)$$

where $\mathbf{v}[\mathbf{r}_j(t)]$ is the local velocity of the particle at position $\mathbf{r}_j(t)$, \mathbf{q}_b and \mathbf{q}_g are the photon momentum transfer vectors for the blue light and the green light, respectively. Because of the random distribution of the particles in the fluid, the fluctuation terms in Eq. (4) may also be dropped, and the remaining terms must satisfy the condition $\mathbf{q}_b \cdot [\mathbf{r}_i(0) - \mathbf{r}_j(0)] + \mathbf{q}_g \cdot [\mathbf{r}_k(0) - \mathbf{r}_l(0)] = 0$. The possible choices to satisfy the condition are (1) $i = j = k = l$, for arbitrary nonzero \mathbf{q}_b and \mathbf{q}_g ; (2) $i = j \neq k = l$, for arbitrary nonzero \mathbf{q}_b and \mathbf{q}_g ; (3) $i = l \neq j = k$, for $\mathbf{q}_b = \mathbf{q}_g \neq 0$; and (4) $i = k \neq j = l$, for $\mathbf{q}_b = -\mathbf{q}_g \neq 0$.

Equation (2) then becomes

$$g_c(t) = \frac{\langle N(0)N(t) \rangle \langle A(0)A(t) \rangle}{\bar{N}^2 \bar{A}^2} + \frac{1}{\bar{N}^2 \bar{A}^2} \times \sum_{i \neq j} \langle \alpha_{if}^i(0) \alpha_{if}^j(t) \alpha_{if}^j(0) \alpha_{if}^i(t) \rangle F(\mathbf{q}, t), \quad (5)$$

where $N(t)$ is the number of particles in the scattering volume, $A(t) [= \alpha_{if}^2(t)]$ is the scattering power of the particle, and

$$F(\mathbf{q}, t) = \langle e^{-i\mathbf{q}\cdot \int_0^t dt' \{ \mathbf{v}[\mathbf{r}_k(t')] - \mathbf{v}[\mathbf{r}_i(t')] \}} \rangle. \quad (6)$$

The condition $i = j = k = l$ gives rise to the first term in Eq. (5), and the conditions $i = l \neq j = k$ and $i = k \neq j = l$ result in the same function, which is the second term in Eq. (5).

To get Eq. (5) we have made following assumptions. (1) There is no orientational correlation between particles in the dilute solution [$\langle \alpha_{if}^i(0) \alpha_{if}^j(t) \rangle = 0$ for $i \neq j$]. Therefore, all the terms in Eq. (4), which satisfy the condition $i = j \neq k = l$, may also be dropped. This assumption is certainly valid for rotational diffusion in thermal equilibrium, but it remains to be checked for turbulent fluid motions. (2) The number of particles in the scattering volume changes with time, which is statistically independent of $A(t)$.

The cross-correlation function $g_c(t)$ in Eq. (5) can be rewritten as

$$g_c(t) \simeq 1 + g_N(t) + g_A(t) + g_{\text{coh}}(\mathbf{q}_b = \pm \mathbf{q}_g; t), \quad (7)$$

with $g_N(t) = \langle \delta N(0) \delta N(t) \rangle / \bar{N}^2$, $g_A(t) = \langle \delta A(0) \delta A(t) \rangle / \bar{A}^2$, and $g_{\text{coh}}(\mathbf{q}_b = \pm \mathbf{q}_g; t)$ being the second term in Eq. (5). Here $\delta N(t) = N(t) - \bar{N}$ and $\delta A(t) = A(t) - \bar{A}$. Since in a typical experimental arrangement the particle number in the scattering volume can be controlled in the range $1 < \bar{N} < 100$, a second order term ($\sim 1/\bar{N}^2$) in Eq. (7) is ignored. The coherent correlation function $g_{\text{coh}}(\mathbf{q}_b = \pm \mathbf{q}_g; t)$ is a product of two correlation functions; one is for the amplitude fluctuations and the other is for the phase fluctuations of the scattered light. The phase fluctuations arise from the interference between the coherent fields scattered by different moving particles, and thus $F(\mathbf{q}, t)$ equals to zero if the condition $\mathbf{q}_b = \pm \mathbf{q}_g$ is not met. Under the condition $\mathbf{q}_b = \pm \mathbf{q}_g$, there is only one photon momentum transfer vector (\mathbf{q}) involved, so that the subscripts b and g are dropped in Eq. (6). Notice that the amplitude of $g_{\text{coh}}(\mathbf{q}_b = \pm \mathbf{q}_g; t)$ is essentially 1, while $g_N(t)$ and $g_A(t)$ go as $1/\bar{N}$. Another important difference between $g_{\text{coh}}(\mathbf{q}_b = \pm \mathbf{q}_g; t)$ and $g_N(t)$ [or $g_A(t)$] is that the "translational factor" $F(\mathbf{q}, t)$ is a function of \mathbf{q} , but $g_N(t)$ and $g_A(t)$ are purely local in character and hence do not depend on \mathbf{q} .

Experimentally, one can measure $g_{\text{coh}}(\mathbf{q}_b = \pm \mathbf{q}_g; t)$ using either the autocorrelation method⁷ with $\mathbf{q}_b = \mathbf{q}_g$, or the cross-correlation scheme¹¹⁻¹⁴ under the condition $\mathbf{q}_b = -\mathbf{q}_g$. In both cases, one should keep $\bar{N} \gg 100$. [The new correlator to be used in the experiment can pick up contributions from $g_N(t)$ or/and $g_A(t)$ when $\bar{N} < 100$.] Notice that even in the limit $\bar{N} \gg 100$, the overall particle concentration may still be very low, so that the particle interaction and the multiple scattering effects can be ignored. The function $g_N(t)$ can be obtained under the conditions $\mathbf{q}_b \neq \pm \mathbf{q}_g$ and $\bar{N} < 100$. Optically isotropic spherical particles (which are commercially available in various sizes) should be used, so that the measured correlation function is not sensitive to the rotational motion of the probe particles [$g_A(t) = 0$]. The function $g_A(t)$ can be obtained under the same conditions. However, optically *anisotropic* particles should be used in this case, and the time scales for $g_A(t)$ must be well separated from those for $g_N(t)$, since the measured $g_c(t) = 1 + g_N(t) + g_A(t)$.

Measurements of $g_{\text{coh}}(\mathbf{q}_b = \pm \mathbf{q}_g; t)$ have been especially fruitful in studies of diffusive motion of small particles,^{7,8} fluid dynamics in laminar¹⁶ and turbulent¹⁷ flows, and the number fluctuations for Brownian particles and motile microorganisms.^{15,18-22} The correlation function $g_{\text{coh}}(\mathbf{q}_b$

$= \pm \mathbf{q}_g; t)$ is also utilized to probe the rotational diffusion of small particles suspended in a solution.^{4,5,7} This can be done when the translational motion of the particles is exactly known. An example is the translational and rotational motions of Brownian particles in a thermal equilibrium solution. In this case $F(\mathbf{q}, t) = e^{-2Dq^2 t}$, and $g_{\text{coh}}(\mathbf{q}_b = \pm \mathbf{q}_g; t)$ has the following forms:⁷

$$g_{\text{coh}}^{VH}(\mathbf{q}_b = \pm \mathbf{q}_g; t) = e^{-(12\Theta + 2Dq^2)t}, \quad (8)$$

and

$$g_{\text{coh}}^{VV}(\mathbf{q}_b = \pm \mathbf{q}_g; t) = \frac{\{1 + (4/45)(\beta/\alpha)^2 e^{-6\Theta\tau}\}^2}{\{1 + (4/45)(\beta/\alpha)^2\}^2} e^{-2Dq^2 t} \simeq e^{-2Dq^2 t}, \quad (9)$$

when the *VH* and *VV* scattering geometries are used, respectively. In the above, $\beta \equiv (\alpha_{\parallel} - \alpha_{\perp})$ and $\alpha \equiv (\alpha_{\parallel} + 2\alpha_{\perp})/3$, with the molecular polarizability tensor being assumed to be of cylindrical symmetry with a molecular-fixed polarizability component α_{\parallel} parallel to its symmetry axis and α_{\perp} in any direction perpendicular to this axis. In the last equality of Eq. (9), the ratio β/α is assumed to be small. The rotational diffusion constant Θ and the translational diffusion constant D have been calculated for spherical and rodlike particles.⁷

B. Rotations of small particles in laminar flows

The discussion on the scattering amplitude fluctuations in the above section is general; either rotations of optically anisotropic particles or internal motions of flexible molecules can produce such fluctuations. Here we focus on the rotation of small particles in a steady laminar flow. The molecular polarizability tensor of the probe particles is assumed to be of cylindrical symmetry. It has been shown⁷ that the correlation function $g_A(t)$ has the following forms:

$$g_A^{VH}(t) = \frac{(2\pi)^2}{\bar{N}} [F_{1,1}^{(2)}(t) + F_{1,-1}^{(2)}(t) + F_{-1,1}^{(2)}(t) + F_{-1,-1}^{(2)}(t)]^2, \quad (10)$$

and

$$g_A^{VV}(t) = \frac{1}{\bar{N}} \frac{[1 + (16\pi/45)(\beta/\alpha)^2 F_{0,0}^{(2)}(t)]^2}{[1 + (4/45)(\beta/\alpha)^2]^2}. \quad (11)$$

In the above, the orientational correlation function

$$F_{m,m'}^{(l)}(t) = \int d^2\mathbf{u}_0 \int d^2\mathbf{u} Y_{lm}(\mathbf{u}) P(\mathbf{u}, t; \mathbf{u}_0, 0) \times K(\mathbf{u}_0) Y_{lm'}^*(\mathbf{u}_0), \quad (12)$$

where the $Y_{lm}(\mathbf{u})$ are the spherical harmonics, and $P(\mathbf{u}, t; \mathbf{u}_0, 0)$ is the probability density function for a particle having orientation \mathbf{u} at time t given that it had orientation \mathbf{u}_0 initially. The function $K(\mathbf{u}_0) = 1/(4\pi)$ is the probability distribution of initial orientations of the probe particles, and it is assumed to be of uniform distribution. The orien-

tation of an optically anisotropic particle is specified by a unit vector \mathbf{u} directed along the optical axis of the particle with spherical polar coordinates (θ, ϕ) .

Further calculation of $g_A(t)$ thus reduces to the determination of the function $P(\mathbf{u}, t; \mathbf{u}_0, 0)$, which reflects how the angles $\theta(t)$ and $\phi(t)$ change with time. For small particles in a steady laminar flow, $P(\mathbf{u}, t; \mathbf{u}_0, 0)$ can be calculated by solving the convective rotational diffusion equation. Since the orientation vector \mathbf{u} can be regarded as a point on a unit sphere, rotational diffusion of \mathbf{u} can be treated as translational diffusion of the end point of \mathbf{u} on the unit sphere. Therefore, we have

$$\left[\frac{\partial}{\partial t} + (\mathbf{v}_u \cdot \nabla_u) \right] P(\mathbf{u}, t; \mathbf{u}_0, 0) = \Theta \nabla_u^2 P(\mathbf{u}, t; \mathbf{u}_0, 0), \quad (13)$$

where \mathbf{v}_u is the linear velocity of the end point on the surface of the unit sphere, Θ is the rotational diffusion constant of the seed particles, and the subscript u indicates the constraint on the unit sphere.

In the spherical coordinate system Eq. (13) becomes

$$\frac{\partial P(\mathbf{u}, t; \mathbf{u}_0, 0)}{\partial t} = -[i\Omega \hat{I}_z + \Theta \hat{I}^2] P(\mathbf{u}, t; \mathbf{u}_0, 0), \quad (14)$$

where

$$\hat{I}^2 = -\frac{1}{\sin^2 \theta} \left[\sin \theta \frac{\partial}{\partial \theta} \left(\sin \theta \frac{\partial}{\partial \theta} \right) + \frac{\partial^2}{\partial \phi^2} \right], \quad (15)$$

and

$$\hat{I}_z = -i \frac{\partial}{\partial \phi}. \quad (16)$$

In the above, \hat{I} is the total angular momentum operator in the quantum mechanics, \hat{I}_z is the z component of \hat{I} , and Ω is the amplitude of the angular velocity $\boldsymbol{\Omega}$ of the particle. The direction of $\boldsymbol{\Omega}$ is assumed to be along the z axis parallel to the incident polarization. The final solution of Eq. (14) is

$$P(\mathbf{u}, t; \mathbf{u}_0, 0) = \sum_{l,m} e^{-[i\Omega m + \Theta l(l+1)]t} Y_{lm}(\mathbf{u}_0) Y_{lm}^*(\mathbf{u}). \quad (17)$$

With Eqs. (17) and (12), we have the final results

$$g_A^{VH}(t) = \frac{1}{\bar{N}} e^{-12\Theta t} \cos^2(\Omega t), \quad (18)$$

and

$$g_A^{VV}(t) = \frac{1}{\bar{N}} \frac{[1 + (4/45)(\beta/\alpha)^2 e^{-6\Theta\tau}]^2}{[1 + (4/45)(\beta/\alpha)^2]^2}. \quad (19)$$

Equations (18) and (19) show that an appreciable amount of the depolarized scattering light is needed in order to measure the rotation of the probe particles. It is seen that $g_A^{VV}(t)$ will not decay much if the ratio β/α is small. On the other hand, $g_A^{VH}(t)$ has a relatively large signal-to-noise ratio. Equation (18) can be used to measure the magnitude of the local vorticity, $\boldsymbol{\omega} = \nabla \times \mathbf{v}$, in a steady laminar flow with a stream velocity \mathbf{v} . The vorticity is obtained using the

fact that *spherical* particles rotate at a frequency, Ω , accurately equal to half the vorticity ($\omega=2\Omega$).^{6,23} To accomplish this it is necessary to seed the flow with particles which are spherical in shape but scatter light anisotropically. Eq. (18) is useful to measure the convective rotation rate of the probe particles only when Ω is larger than 6Θ . This can be achieved by choosing large particles, since Θ is inversely proportional to the cube of the size of the particles.⁷ It is also seen from Eq. (19) that $g_A^{VV}(t)$ is not sensitive to the hydrodynamic flow. This is because the direction of Ω is assumed to be along the z axis parallel to the incident polarization. Perhaps it is more interesting to measure the local vorticity ω in a turbulent flow, in which both the magnitude and the direction of ω change with time. We will address the issue in a separate paper.²⁴

C. Number fluctuations in flow systems

The correlation function $g_N(t)$ for number fluctuations can be written as²²

$$g_N(t) = \frac{1}{\bar{N}} \frac{\int d^3\mathbf{r} \int d^3\mathbf{r}_0 I(\mathbf{r}) I(\mathbf{r}_0) P(\mathbf{r}-\mathbf{r}_0;t)}{[\int d^3\mathbf{r} I(\mathbf{r})]^2}, \quad (20)$$

where $P(\mathbf{r}-\mathbf{r}_0;t)$ is the probability density function for a particle to move from \mathbf{r}_0 to \mathbf{r} in a time t , and $I(\mathbf{r})$ is the light intensity profile. In a typical laser scattering experiment, the scattering volume has a thin cylindrical shape with the length L of the cylinder being much larger than its waist radius σ . Therefore, the intensity profile has the form

$$I(\mathbf{r}) = I_0 e^{-2(r_\perp/\sigma)^2}, \quad (21)$$

where r_\perp is the radial distance from the center of the laser beam, and I_0 is the light intensity at the center of the beam. Equation (21) assumes that the intensity distribution in the direction of the beam propagation is uniform, and that in the perpendicular direction it is Gaussian.

The probability density function $P(\mathbf{r}-\mathbf{r}_0;t)$ characterizes the dynamics of the probe particles in the fluid. For Brownian particles with a uniform initial particle distribution, $P(\mathbf{r}-\mathbf{r}_0;t)$ has the form^{15,18,22}

$$P(\mathbf{r}-\mathbf{r}_0;t) = \frac{e^{-(\mathbf{r}-\mathbf{r}_0)^2/(4Dt)}}{(4\pi Dt)^{3/2}}, \quad (22)$$

and

$$g_N(t) = \frac{1}{\bar{N}(1+4Dt/\sigma^2)}. \quad (23)$$

It is seen from Eq. (23) that the characteristic decay time of $g_N(t)$ is the time taken by a particle to diffuse a distance of σ . This time (σ^2/D) is of the order of seconds for typical values of σ and D . It is much larger than the characteristic decay time (Dq^2)⁻¹ for $g_{\text{coh}}(\mathbf{q}_b = \pm \mathbf{q}_g; t)$ in Eq. (9) (typically between ms and μ s, the time taken by a particle to diffuse a distance comparable to the wavelength of the incident light).

When the particles in the scattering volume have a uniform velocity \mathbf{v} , the function $P(\mathbf{r}-\mathbf{r}_0;t)$ takes the form²²

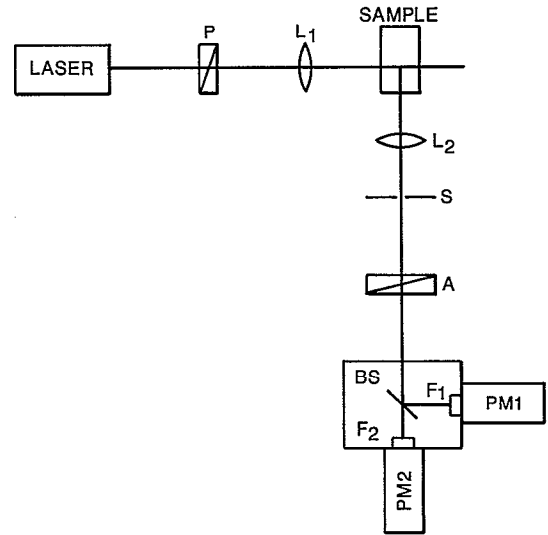


FIG. 2. Schematic diagram of the experimental setup: P , polarizer; L_1 , L_2 , lenses; S , adjustable slit; A , analyzer; PM1, PM2, photomultipliers; BS, beam splitter; F_1 , F_2 , interference filters.

$$P(\mathbf{r}-\mathbf{r}_0;t) = \delta[(\mathbf{r}-\mathbf{r}_0) - \mathbf{v}t], \quad (24)$$

and then

$$g_N(t) = (1/\bar{N}) e^{-(\mathbf{v}t/\sigma)^2}. \quad (25)$$

For turbulent flows we have

$$g_N(t) = \frac{1}{\bar{N}} \int dv P(v) e^{-(\mathbf{v}t/\sigma)^2}, \quad (26)$$

where $P(v)$ is the probability density function of the local velocity v perpendicular to the direction of the beam propagation. The spatial resolution for the local velocity measurement is determined by the scattering volume viewed by a photodetector. In a typical experimental arrangement, the length L of the scattering volume can be controlled below 100 μ m. By changing the direction of the incident laser beam, one can measure the local velocity in different directions. The beam waist radius σ can be calibrated using Eq. (23) when the flow is absent. Besides its advantages of high spatial resolution, fast temporal response, and ease of use, the technique has a sampling rate much faster than that of laser Doppler velocimetry (LDV). This is because the present technique may allow ~ 100 particles in the scattering volume, whereas the LDV method only allows one particle in the scattering volume at any given time.

III. EXPERIMENT

Figure 2 shows the experimental setup. The lens L_1 focused the incident beam from a 4-W argon-ion laser (Coherent Innova-304) to form a thin cylindrically shaped scattering volume in the sample solution. The focal length (f) of L_1 was 34 mm, and the incident beam radius (σ_0) was 0.8 mm. This combination should give a focal spot radius $\sigma \approx 0.6f\lambda/\sigma_0 \approx 13 \mu$ m. The beam radius is a very sensitive parameter to control the scattering volume

viewed by photodetectors. The laser was under multiline operation with a wavelength range from 457.9 nm to 514.5 nm. The laser intensity was regulated under the light regulation and the power track modes. The maximum variation of the peak intensity was below 0.5% in a half-hour period.²⁵ The stability of laser light is important in measuring the scattering amplitude fluctuations with long relaxation times. The lens L_2 imaged the laser beam in the sample cell without a magnification onto a slit S of variable width from 0.01 to 3 mm. Light passing through the slit S fell on the photomultipliers, which recorded the time-varying intensities. The polarizer P in front of the laser ensured that the incident light was vertically polarized, and the analyzer A allowed either horizontally polarized light (VH scattering geometry) or vertically polarized light (VV scattering geometry) to go through. The two photomultipliers PM1 and PM2 were mounted at right angles on a cubic box, which was located behind the analyzer. The beam splitter BS in the center of the cubic box had a reflection-to-transmission ratio of 50/50. An interference filter (F_1 or F_2) was placed in front of each of the photomultipliers. These filters had a bandwidth (FWHM) of 1 nm. The spectral line for F_1 was 488 nm, and that for F_2 was 514.5 nm.

The TTL pulse trains from the two photomultipliers were fed to the correlator, whose output gives the cross-correlation function

$$g_c(t) = \frac{\langle I_b(t')I_g(t'+t) \rangle}{\langle I_b \rangle \langle I_g \rangle} = 1 + bG_c(t), \quad (27)$$

where I_b is the intensity of the blue light ($\lambda=488$ nm), I_g is the intensity of the green light ($\lambda=514.5$ nm), and b is an instrumental constant which depends on the geometry of the experimental setup. Because there is no phase coherence between the blue light and the green light, the measured $G_c(t) = g_N(t) + g_A(t)$. The correlation function $g_A(t) = 0$, when optically isotropic spherical particles are used. Measurements of $g_c(t)$ were made at room temperature. The ALV-5000 multiple- τ correlator was used to measure $g_c(t)$ with a fixed range of lag times between 0.2 μ s and 1 h. An optimum statistical accuracy over the whole range of lag times was ensured by 31 sample times and 8×8 bit or 16×16 bit processing into 256 channels (almost-logarithmic spaced in time) of 64 bit depth.²⁶

The sample cell was a standard cuvette, 1 cm \times 1 cm in cross section and 6 cm in high. It was filled with a dilute aqueous suspension of probe particles. The volume fraction of the particles was below 10^{-5} . We have verified that in this particle concentration range, the particle interaction can be ignored. In the test of the technique itself, we first studied Brownian rotation of the polytrafluoroethylene (PTFE) latex particles. The PTFE particles were synthesized by a dispersion polymerization process, which, in the presence of the emulsifier, yields stable aqueous latexes.²⁷ The latex particles thus formed possess a crystalline structure and optical anisotropy.^{28,29} Such a colloidal suspension is ideal for the investigation attempted here. With the electron microscope we find that the PTFE particles have a rodlike shape with an average length 0.45 μ m and an

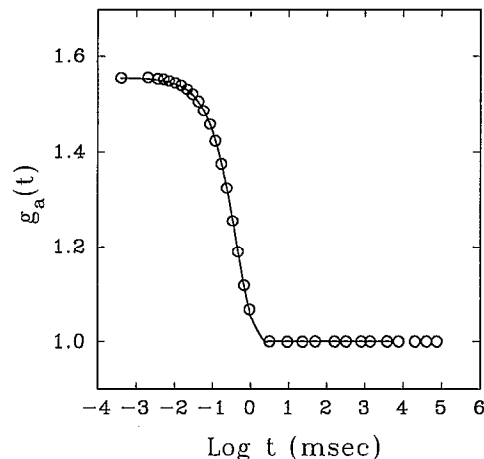


FIG. 3. The measured autocorrelation function $g_a(t)$ as a function of $\log t$ for the PTFE particles. The measurement was made at $\theta=90^\circ$ and with the VH scattering geometry. The solid curve is a fit to $1 + be^{-2\Gamma t}$ with $\Gamma=1.16$ ms^{-1} and $b=0.56$.

average diameter 0.19 μ m. The particles are relatively monodispersed with an average polydispersity of 16% (the standard deviation over the average length). To further characterize these particles, we also measured the intensity autocorrelation function

$$g_a(t) = \langle I(t')I(t'+t) \rangle / \langle I \rangle^2 = 1 + bG_a(t), \quad (28)$$

where $I(t)$ is the scattering intensity. The measured $G_a(t)$ is just the coherent correlation function $g_{\text{coh}}(\mathbf{q}_b = \pm \mathbf{q}_g; t)$, which is calculated in Eqs. (8) and (9). The experimental setup was the same as shown in Fig. 2, except only one photomultiplier was used. Measurements were made at the scattering angles from 20° to 150° .

IV. RESULTS

Figure 3 shows the measured $g_a(t)$ as a function of $\log t$ for the PTFE particles. The measurement was made at $\theta=90^\circ$ and with the VH scattering geometry. The solid curve is a fit to $1 + be^{-2\Gamma t}$, from which we obtain the decay rate $\Gamma=1.16$ ms^{-1} and $b=0.56$. According to Eqs. (8) and (9), the decay rate $\Gamma_{VH}=6\Theta + Dq^2$ in the VH scattering geometry and $\Gamma_{VV}=Dq^2$ in the VV scattering geometry. Figure 4 shows the measured Γ as a function of q^2 for the two scattering geometries. The solid lines are linear fits to the data points. The two fitted lines have the same slope, from which we find $D=1.8 \times 10^{-8}$ cm^2/s . As we expected, the intercept of the lower solid line is zero. From the intercept for the VH scattering geometry, we obtain $\Theta=41 \pm 6$ s^{-1} . The obtained values of D and Θ agree satisfactorily with previous measurements by Piazza *et al.*²⁸ Using the formulas for the diffusion constants of rodlike particles,⁷ we find that the length of the PTFE particles equals 0.46 μ m, with the aspect ratio of the particle diameter to the length being 0.42. This result agrees well with the electron microscopic observation, as discussed in Sec. III.

Figure 5 shows the measured cross-correlation function $g_c(t)$ vs t for the dilute PTFE aqueous suspension in

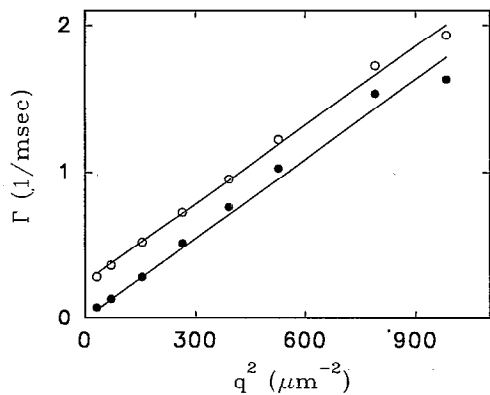


FIG. 4. The measured decay rate Γ as a function of q^2 in both the VH scattering geometry (open circles) and the VV scattering geometry (solid circles). The solid lines are fits to $a_1 + a_2 q^2$, with $a_1 = 0.246$, $a_2 = 0.00179$ for the upper solid line, and $a_1 = 0$, $a_2 = 0.0018$ for the lower solid line.

the VH scattering geometry [Fig. 5(a)] and in the VV scattering geometry [Fig. 5(b)]. In our measurements the typical signal-to-noise ratio [evaluated by the value of $g_c(t) - 1$ at time $t = 0$] for $g_c(t)$ is in the range between 10% and 1%, which is very small compared with 56% for $g_a(t)$ (see Fig. 3). Nevertheless, the ALV-5000 correlator

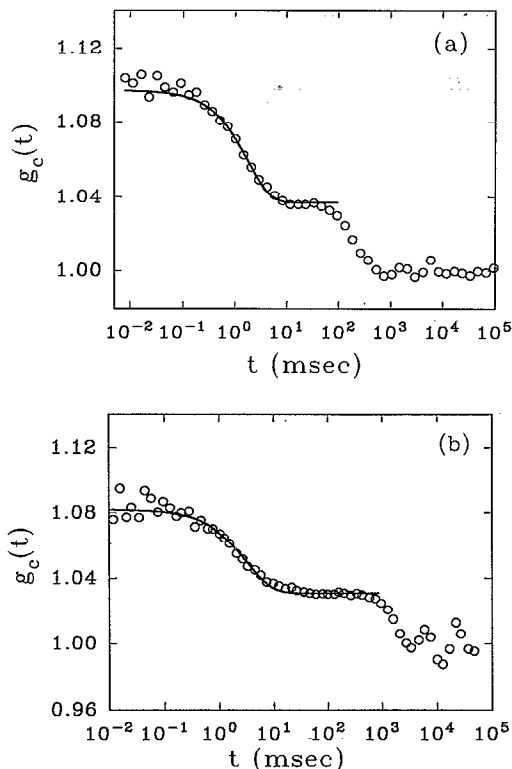


FIG. 5. The measured cross-correlation function $g_c(t)$ as a function of t for the PTFE particles (a) in the VH scattering geometry and (b) in the VV scattering geometry. The measurements were made at $\theta = 90^\circ$. The fitted functional forms are $1.037 + 0.06 \exp(-t/1.8 \text{ ms})$ [the solid curve in (a)], and $1.004 + 0.027[1 + 0.7 \exp(-t/3.8 \text{ ms})]^2$ [the solid curve in (b)].

is capable of measuring such small intensity fluctuations. In fact, using the ALV-5000 correlator we were able to measure fluctuating signals with a signal-to-noise ratio as low as 0.1%. It is seen that there are two decay modes in Fig. 5. The slow decay is caused by number fluctuations of the particles in the scattering volume, and will be discussed later. The fast decay in Fig. 5 is produced by Brownian rotations of the PTFE particles. The solid curve in Fig. 5(a) is the fitted form $1.037 + 0.06 \exp(-t/1.8 \text{ ms})$, and using Eq. (18) (with $\Omega = 0$) we find $\Theta = 46 \pm 6 \text{ s}^{-1}$. The solid curve in Fig. 5(b) is the fitted form $1.004 + 0.027[1 + 0.7 \exp(-t/3.8 \text{ ms})]^2$, from which we obtain $\Theta = 44 \pm 6 \text{ s}^{-1}$ [see Eq. (19)]. These values of Θ agree with the measurements in Fig. 4. Figure 5 thus demonstrates that incoherent cross-correlation spectroscopy is capable of measuring the pure scattering amplitude fluctuations whereas the fast phase fluctuations of the scattered light are eliminated.

We now discuss the differences between $g_A^{VH}(t)$ and $g_A^{VV}(t)$. As shown in Eq. (19), the isotropic scattering (proportional to α^2) in the VV geometry contributes a background signal to $g_A^{VV}(t)$. Such a background signal usually reduces the signal-to-noise ratio for measurements of $g_A^{VV}(t)$. This effect is not pronounced in Fig. 5(b) because of the relative large value of β/α for our PTFE crystalline particles. By comparing Eq. (18) with Eq. (19), one finds that the functional form of $g_A^{VV}(t)$ is more complicated, and an additional fitting parameter (β/α) is needed in order to fit the measured $g_A^{VV}(t)$. In fact, we used four fitting parameters for the solid fitting curve in Fig. 5(b). The first two amplitudes (i.e., 1.004 and 0.027) in the fitting curve have large uncertainties. Since the scattering in the VV geometry is strong, one normally does not need much laser power to measure $g_A^{VV}(t)$. A small laser power can reduce the local laser heating, which may introduce a convection flow in the sample cell. As will be discussed below, a small convection flow can cause a noticeable change in the decay of $g_N(t)$. In fact, such an effect can be seen in Fig. 5. The slow decay mode in Fig. 5(a) shows a larger decay rate than that in Fig. 5(b). This is because the incident laser intensity in the VH geometry [Fig. 5(a)] is stronger than that in the VV geometry [Fig. 5(b)], and the laser heating enhances the particle number fluctuations.

To study the particle number fluctuations in the scattering volume, we measured $g_c(t)$ in the identical cell, but with the PTFE rodlike particles replaced with polystyrene latex spheres of various diameters. These latex spheres are optically isotropic scatterers, and the measurements were made in the VV scattering geometry. Figure 6(a) shows the measured $g_c(t)$ vs $\log t$ for the latex spheres of diameter $0.14 \mu\text{m}$. For comparison, we also measured $g_a(t)$ for the same latex particles [Fig. 6(b)]. It is seen from Fig. 6 that the translational diffusion of the particles contributes a fast decay mode to $g_a(t)$. This fast mode is absent in the measured $g_c(t)$ because the incoherent detecting method was used. The solid curves in Fig. 6 are the fitted forms $1.0 + 0.011 \exp(-t/18.5 \text{ s})$ [Fig. 6(a)] and $1.0 + 0.025 \exp(-t/19.5 \text{ s}) + 0.027 \exp(-t/0.315 \text{ ms})$ [Fig. 6(b)]. From the fast decay time $\tau_f = 1/(2 Dq^2) = 0.315$

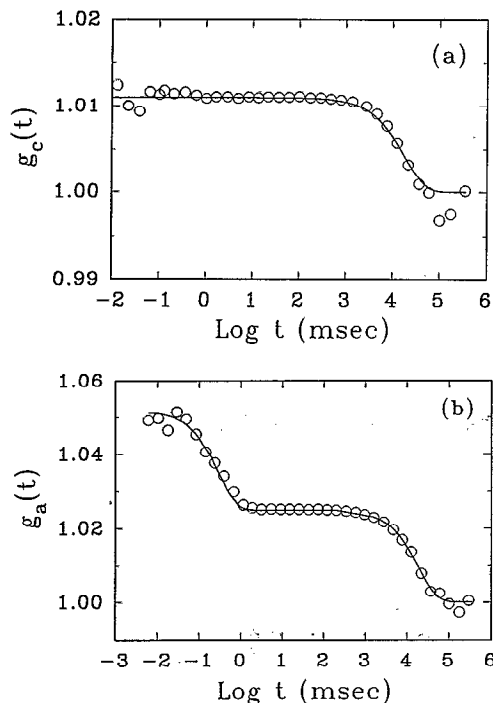


FIG. 6. The measured cross-correlation function $g_c(t)$ (a) and the auto-correlation function $g_a(t)$ (b) as a function of $\log t$ for the polystyrene latex spheres of diameter $0.14 \mu\text{m}$. The measurements were made at $\theta=90^\circ$ and with the VV scattering geometry. The fitted functional forms are $1.0+0.011 \exp(-t/18.5 \text{ s})$ [the solid curve in (a)], and $1.0+0.025 \exp(-t/19.5 \text{ s})+0.027 \exp(-t/0.315 \text{ ms})$ [the solid curve in (b)].

ms, we obtain the diffusion constant $D=3.0 \times 10^{-8} \text{ cm}^2/\text{s}$ and the expected value of the particle diameter.

With the measured slow decay time $\tau_s=18.5 \pm 4 \text{ s}$ and the diffusion constant D , we calculate the beam waist radius $\sigma = \sqrt{4 D \tau_s} = 14.9 \mu\text{m}$ [see Eq. (23)]. This beam waist radius is consistent with our estimated value of $13 \mu\text{m}$. The σ^2 dependence of τ_s has also been verified experimentally. We find that the decay time τ_s is increased four times when the focal length f of L_1 is doubled. It should be pointed out that the functional form of the measured $g_N(t)$ in Fig. 6 is exponential-like, which is different from the calculated one in Eq. (23). At short delay time t , the two functions are indistinguishable, but the measured $g_N(t)$ decays faster than that shown in Eq. (23) at large delay times. One possible reason for this deviation is the non-Gaussian beam profile. A Gaussian beam profile is assumed in obtaining Eq. (23). In the experiment we used a diaphragm to reduce the diameter of the incident beam. Chromatic aberrations of the simple lens (L_1) used in the measurements may also affect the beam profile. It is found that the measured $g_N(t)$ is extremely sensitive to the convection flow produced by the laser heating and even the nearby air current. In the experiment the sample cell was covered by a styrofoam box to minimize the air current, and a small laser power ($\sim 20 \text{ mW}$) was used to reduce the laser heating.

As shown in Eqs. (23) and (25), the amplitude of $g_N(t)$ is proportional to $1/\sqrt{N}$. This is true when the scattered field obeys Gaussian statistics. If the fluctuations of

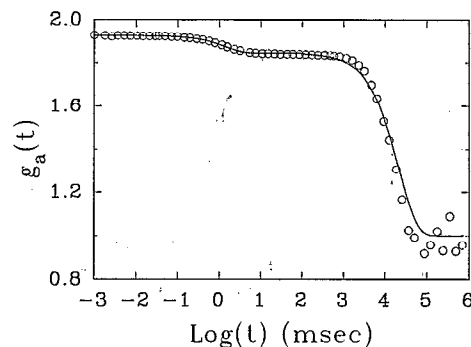


FIG. 7. The measured autocorrelation function $g_a(t)$ as a function of $\log t$ for the polystyrene latex spheres of diameter $0.64 \mu\text{m}$. The measurement was made at $\theta=90^\circ$ and with the VV scattering geometry. The solid curve is the fitted form $1.0+0.84 \exp(-t/21 \text{ s})+0.079 \exp(-t/1.34 \text{ ms})$.

the scattered field is highly non-Gaussian, the amplitude $g_N(t=0)=\langle I^2 \rangle / \langle I \rangle^2$ can be much larger than 1 (enhanced fluctuations).¹⁵ Figure 7 shows the plot of the measured $g_a(t)$ vs $\log t$ for the polystyrene latex spheres of diameter $0.64 \mu\text{m}$. The fast decay mode is due to the translational diffusion of the latex particles, and the slow one is caused by the number fluctuations of particles in the scattering volume. The measured $g_N(t)$ (slow decay mode) in Fig. 7 has a much larger amplitude than those in Fig. 6. For the measurement in Fig. 7, there were only a few latex spheres of diameter $0.64 \mu\text{m}$ in the scattering volume (large particles were used to increase the scattering power). Fluctuations of the scattering intensity are found to be non-Gaussian, and their probability density function has a long tail at the large intensity side. For the measurements in Fig. 6, on the other hand, the number of particles in the scattering volume was approximately 100, and the probability density function of the scattering intensity has a nice Gaussian form. The solid curve in Fig. 7 is the fitted form $1.0+0.84 \exp(-t/21 \text{ s})+0.079 \exp(-t/1.34 \text{ ms})$.

As discussed in Sec. II, $g_N(t)$ can be used to measure the flow velocity. The technique is tested in a laminar Poiseuille flow. The flow experiment was carried out in a rectangular cell with the dimensions shown in Fig. 8. The

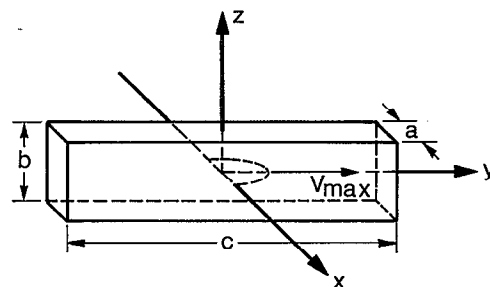


FIG. 8. The rectangular flow cell and the scattering geometry. The cell was made of quartz, and has the following dimensions: $a=0.1 \text{ cm}$, $b=1.2 \text{ cm}$, and $c=5 \text{ cm}$. The flow was in the y direction, and the incident laser beam was along the x axis with the polarization in the z direction. The scattering angle $\theta=45^\circ$, which bisected the angle between the x axis and the y axis.

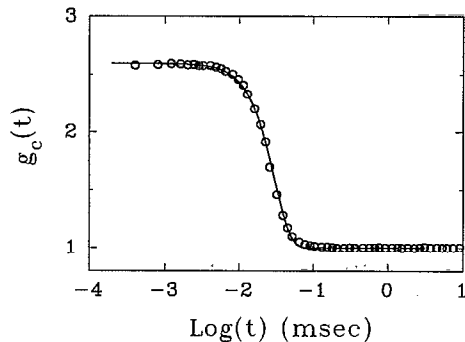


FIG. 9. The measured cross-correlation function $g_c(t)$ as a function of $\log t$ at $V_0=41.0$ cm/s. The solid curve is a fit to $1+b \exp[-(\Gamma t)^2]$, with $b=1.59$ and $\Gamma=33.3$ ms $^{-1}$.

flow was in the y direction, and the incident laser beam was along the x axis with the polarization in the z direction. The scattering angle $\theta=45^\circ$, which bisected the angle between the x axis and the y axis. Because of the large aspect ratio of the cell, $b/a=12$, the dominant velocity gradient was in the x direction. For the Poiseuille flow the velocity profile in the x direction has a parabolic form, and the flow velocity at the center of the cell $V_0=3J/(2ab)$, with J being the flow rate. The slit S of width 0.3 mm (see Fig. 2) was aligned, such that the photomultipliers could only see the scattering from the midpoint of the flow cell. In this way our measurements were most sensitive to the velocity V_0 . Using a magnetically coupled pump (Micropump Model 1316SS), an aqueous solution of the polystyrene spheres of diameter $0.64 \mu\text{m}$ was pumped through the cell at a constant rate J . A maximum velocity $V_0=82.5$ cm/s could be achieved with this apparatus, and the corresponding Reynolds number $\text{Re}=V_0 a/\nu \approx 825$. This Reynolds number is well below the turbulent transition Reynolds number for Poiseuille flows.³⁰ Thus the experiment was in the laminar-flow regime.

Figure 9 shows the measured $g_c(t)$ as a function of $\log t$ at $V_0=41.0$ cm/s. The solid curve is a fit to $1+b \exp[-(\Gamma t)^2]$, with $\Gamma=33.3$ ms $^{-1}$ and $b=1.59$. The functional form of the measured $g_c(t)$ agrees well with the calculated one in Eq. (25). Because of the small number of particles in the scattering volume, the scattering shows enhanced fluctuations, which give rise to a large value of b . According to Eq. (25), the decay rate $\Gamma=V_0/\sigma$. Figure 10 shows the plot of the measured Γ vs V_0 for our latex-sphere solution. The measured Γ indeed shows a linear dependence on V_0 , and the solid line in Fig. 10 is a linear fit to the data points. The slope of the straight line is 0.74×10^3 cm $^{-1}$, which gives the beam waist radius $\sigma=13.5 \mu\text{m}$. This result agrees well with our numerical estimation for σ and with the calibration measurements in Fig. 6. Notice that in the above measurements the flow velocity is known, so that the beam waist radius is measured simply as a self-consistent check. In a real flow experiment the local velocity can be obtained from the measured decay rate Γ using Eq. (25). The beam waist radius σ can be calibrated using Eq. (23) when the flow is absent. The smallest velocity

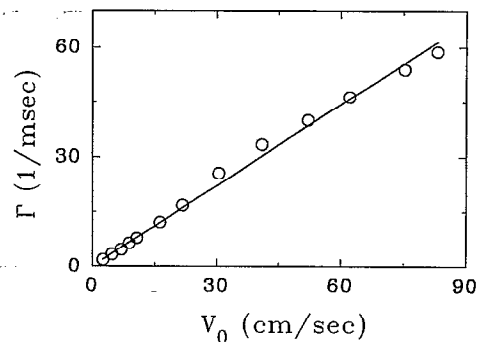


FIG. 10. The measured decay rate Γ as a function of the flow velocity V_0 . The solid line is a linear fit to $\Gamma=(0.74 \times 10^3) V_0$ (s $^{-1}$).

that can be measured using the technique is only limited by the Brownian diffusion of the seed particles. One can slow down the Brownian motion by using large particles. For particles of diameter $0.14 \mu\text{m}$, the limiting velocity can be as small as $\sigma/\tau_s \approx 13 \mu\text{m}/20 \text{ s} = 0.65 \mu\text{m}/\text{s}$. Our technique is particularly useful in the case where the conventional methods, such as hot-wire anemometry and laser Doppler velocimetry (LDV), are not suitable for measuring velocities. An example is turbulent Rayleigh-Bénard convection, in which there are large temperature fluctuations. The strong temperature fluctuations can ruin the calibration of a hot wire anemometer. Fluctuations of the refractive index of the fluid due to the temperature fluctuations may cause the laser beam to dance around in the turbulent fluid, which will perturb the crossing of two laser beams used in LDV.

V. CONCLUSION

Incoherent cross-correlation spectroscopy (ICS) is developed to measure scattering amplitude fluctuations resulting from either internal motions of flexible macromolecules or rotations of rigid particles. With a single-beam two-color cross-correlation scheme, the technique becomes insensitive to rapid phase fluctuations of the scattered light produced by translational motions of the scattering particles. In the theoretical calculation, we consider two common sources which produce the scattering amplitude fluctuations: (1) rotations of optically anisotropic particles in a steady laminar flow and (2) the particle number fluctuations in the scattering volume when a hydrodynamic flow is present. Experimentally, we have examined Brownian rotations of rodlike particles and the particle number fluctuations at thermal equilibrium and in a steady laminar flow. The experiment verifies the theory and demonstrates its applications. Incoherent cross-correlation spectroscopy can be used to measure the magnitudes of the local velocity and the flow vorticity. Such measurements can be made without introducing an invasive probe. The advantages of the technique are its high spatial resolution, fast temporal response, and ease of use. The ICS technique is capable of measuring the scattering amplitude fluctuations with a cut-off frequency up to 1 MHz and a spatial resolution better

than 100 μm . Besides its applications in studies of hydrodynamic flows, we expect the ICS technique to be useful in future for measuring internal motions and shape fluctuations of flexible macromolecules. Measurements of the cross-correlation function will yield information about the fluctuation spectrum of the internal modes of the molecules without predominant contributions from translational motions of these molecules.

ACKNOWLEDGMENTS

We have benefited from fruitful collaborations and illuminating discussions with J. S. Huang, W. I. Goldberg, and K. Schatzel. We thank T. Bellini for providing us the PTFE particles. Thanks are also due to M. Lucas for crucial technical assistance. Acknowledgment is made to the Donors of The Petroleum Research Fund, administered by the American Chemical Society, for the partial support of this work. K.Q.X. acknowledges partial support from Exxon Research and Engineering Company, and the kind hospitality from the Physics Department of Oklahoma State University during his stay. B.J.A. acknowledges the support from the National Science Foundation under Grant No. DMR-9122589.

¹B. Chu, Z. Wang, and J. Yu, *Macromolecules* **24**, 6832 (1991).

²J. S. Huang, S. T. Milner, B. Farago, and D. Richter, *Phys. Rev. Lett.* **59**, 2600 (1987).

³S. T. Milner and S. A. Safran, *Phys. Rev. A* **36**, 4371 (1987).

⁴R. Piazza, V. Degiorgio, M. Corti, and J. Stavans, *Phys. Rev. B* **42**, 4885 (1990).

⁵R. Piazza and V. Degiorgio, *Phys. Rev. Lett.* **67**, 3868 (1991).

⁶M. Frish and W. W. Webb, *J. Fluid Mech.* **107**, 173 (1981).

⁷B. J. Berne and R. Pecora, *Dynamic Light Scattering* (Wiley, New York, 1976).

⁸See, for example, *Photon Correlation Spectroscopy and Velocimetry*, edited by H. Z. Cummins and E. R. Pike (Plenum, New York, 1977).

⁹W. G. Griffin and P. N. Pusey, *Phys. Rev. Lett.* **43**, 1100 (1979).

¹⁰N. A. Clark, B. J. Ackerson, and A. J. Hurd, *Phys. Rev. Lett.* **50**, 1459 (1983).

¹¹B. J. Ackerson, T. W. Taylor, and N. A. Clark, *Phys. Rev. A* **31**, 3183 (1985).

¹²G. D. Phillies, *J. Chem. Phys.* **74**, 260 (1981); *Phys. Rev. A* **24**, 1939 (1981).

¹³J. K. G. Dhont and C. G. De Kruijff, *J. Chem. Phys.* **79**, 1658 (1983).

¹⁴H. J. Mos, C. Pathmamohanarajan, J. K. G. Dhont, and C. G. De Kruijff, *J. Chem. Phys.* **84**, 45 (1986).

¹⁵P. N. Pusey, in *Photon Correlation Spectroscopy and Velocimetry*, edited by H. Z. Cummins and E. R. Pike (Plenum, New York, 1977).

¹⁶G. G. Fuller, J. M. Rallison, R. L. Schmidt, and L. G. Leal, *J. Fluid Mech.* **100**, 555 (1988).

¹⁷P. Tong and W. I. Goldberg, *Phys. Fluids* **31**, 2841 (1988); *Phys. Lett. A* **127**, 147 (1988); P. Tong, W. I. Goldberg, J. S. Huang, and T. A. Witten, *Phys. Rev. Lett.* **65**, 2780 (1990); P. Tong, W. I. Goldberg, and J. S. Huang, *Phys. Rev. A* **45**, 7222 (1991); **45**, 7231 (1991).

¹⁸P. N. Pusey, *J. Phys. A* **12**, 1805 (1979).

¹⁹D. W. Schaefer, *Science* **180**, 1293 (1973).

²⁰W. W. Webb, *Quart. Rev. Biophys.* **9**, 49 (1976).

²¹D. Magde, E. L. Elson, and W. W. Webb, *Biopolymers* **13**, 29 (1974).

²²D. W. Schaefer and B. J. Berne, *Biophys. J.* **15**, 785 (1975).

²³J. B. Jeffery, *Proc. R. Soc. London, Ser. A* **102**, 161 (1922).

²⁴K.-Q. Xia *et al.* (to be published).

²⁵Coherent INNOVA 304 Manual (1991).

²⁶ALV-5000 Multiple- τ Digital Correlator Reference Manual (1989).

²⁷R. H. Ottewill and D. G. Rance, *Colloid Polymer Sci.* **264**, 982 (1986).

²⁸R. Piazza, J. Stavans, T. Bellini, and V. Degiorgio, *Opt. Commun.* **73**, 263 (1989).

²⁹T. Bellini, R. Piazza, C. Sozzi, and V. Degiorgio, *Europhys. Lett.* **7**, 562 (1988).

³⁰D. J. Tritton, *Physical Fluid Dynamics*, 2nd ed. (Oxford, London, 1988).